Biomedicine & Pharmacotherapy 151 (2022) 113163

Contents lists available at ScienceDirect

Biomedicine & Pharmacotherapy

journal homepage: www.elsevier.com/locate/biopha

Butyrate, a postbiotic of intestinal bacteria, affects pancreatic cancer and gemcitabine response in *in vitro* and *in vivo* models

Concetta Panebianco [a], Annacandida Villani [a], Federica Pisati [b], Fabrizio Orsenigo [c], Marynka Ulaszewska [d], Tiziana Pia Latiano [e], Adele Potenza [f], Annapaola Andolfo [d], Fulvia Terracciano [a], Claudio Tripodo [b,g], Francesco Perri [a], Valerio Pazienza [a,*]

[a] Division of Gastroenterology, Fondazione IRCCS Casa Sollievo della Sofferenza, Viale dei Cappuccini, 1, 71013 San Giovanni Rotondo, FG, Italy
[b] Histopathology Unit, Cogentech S.C.a.R.L, Via Adamello, 16, 20139 Milan, MI, Italy
[c] IFOM, FIRC Institute of Molecular Oncology, Milan, Italy
[d] Proteomics and Metabolomics Facility (ProMeFa), IRCCS San Raffaele Scientific Institute, Via Olgettina, 60, 20132 Milan, Italy
[e] Oncology Unit, Fondazione IRCCS "Casa Sollievo della Sofferenza Hospital, Viale dei Cappuccini, 1, 71013 San Giovanni Rotondo, FG, Italy
[f] Dietetic and Clinical Nutrition Unit, Fondazione IRCCS Casa Sollievo della Sofferenza, Viale dei Cappuccini, 1, 71013 San Giovanni Rotondo, FG, Italy
[g] Tumor Immunology Unit, Department of Health Sciences, University of Palermo, Via del Vespro 129, 90127 Palermo, Italy

ARTICLE INFO

Keywords:
Pancreatic cancer
Microbiota
Butyrate
Gemcitabine response

ABSTRACT

Pancreatic ductal adenocarcinoma (PDAC) is an aggressive cancer. The characteristic excessive stromatogenesis accompanying the growth of this tumor is believed to contribute to chemoresistance which, together with drug toxicity, results in poor clinical outcome. An increasing number of studies are showing that gut microbiota and their metabolites are implicated in cancer pathogenesis, progression and response to therapies. In this study we tested butyrate, a product of dietary fibers' bacterial fermentation, whose anticancer and anti-inflammatory functions are known. We provided in vitro evidence that, beside slowing proliferation, butyrate enhanced gemcitabine effectiveness against two human pancreatic cancer cell lines, mainly inducing apoptosis. In addition, we observed that, when administered to a PDAC mouse model, alone or combined with gemcitabine treatment, butyrate markedly reduced the cancer-associated stromatogenesis, preserved intestinal mucosa integrity and affected fecal microbiota composition by increasing short chain fatty acids producing bacteria and decreasing some pro-inflammatory microorganisms. Furthermore, a biochemical serum analysis showed butyrate to ameliorate some markers of kidney and liver damage, whereas a metabolomics approach revealed a deep modification of lipid metabolism, which may affect tumor progression or response to therapy. Such results support that butyrate supplementation, in addition to conventional therapies, can interfere with pancreatic cancer biology and response to treatment and can alleviate some damages associated to cancer itself or to chemotherapy.

1. Introduction

Pancreatic ductal adenocarcinoma (PDAC) is a highly chemo-resistant tumor with a poor prognosis and life expectancy. Only 24% of patients survive 1 year and only 9% will live up to 5 years after diagnosis [1], while the majority of the patients have a life expectancy around 8–13 months [2]. This tremendous scenario is mainly due to the difficulty of attaining an early diagnosis and to the lack of response to the conventional therapies. A hallmark of PDAC is the so called desmoplastic reaction, i. e. the excessive deposition of stroma around the tumor, which is considered responsible of an ineffective drug delivery [3]. Despite recent advances in treatment options, gemcitabine still represents a cornerstone in the management of PDAC [4], although chemo-resistance and drug toxicity further contribute to poor clinical outcome. Therefore, the development of new treatment options endowed with high efficiency and low toxicity supporting conventional approaches is still an unmet need. In the last decade, growing evidences have emerged linking the microbiota to cancer progression and response to therapies, mainly by releasing bioactive microbial metabolic products and by modulating host immune system [5]. Among microbial products,

* Corresponding author.
E-mail address: v.pazienza@operapadrepio.it (V. Pazienza).

https://doi.org/10.1016/j.biopha.2022.113163
Received 15 March 2022; Received in revised form 16 May 2022; Accepted 16 May 2022
Available online 24 May 2022

butyrate, a short chain fatty acid (SCFA) produced by certain bacteria (most of which belonging to the *Firmicutes* phylum) through fibers and carbohydrates fermentation, was described to possess several properties spanning from anti-inflammatory to anti-neoplastic activity [6]. Specifically, in the context of pancreatic cancer, several in vitro studies showed butyrate and its analogs to have pro-differentiating, anti--proliferative, anti-invasive, pro-apoptotic effects in PDAC cell lines [7–9]. These compounds also function as histone deacetylase (HDAC) inhibitors, which are a class of molecules with anti-cancer, anti-inflammatory properties and anti-fibrogenic action [10]. Moreover, chemo-sensitizing effects of butyrate have been demonstrated towards cisplatin, fluorouracil and SN-38 in pancreatic cancer cell lines [11]. As for in vivo studies, sodium butyrate supplementation was described to slow colon cancer growth in non-treated mice and to produce a trend when combined with irinotecan therapy as compared to irinotecan alone [12]. In another mouse model of colon cancer, butyrate was observed to decrease the number of liver metastasis and improve host immune response [13]. Further, sodium butyrate administration decreased tumor volume in a mice model of gastric cancer as compared to control animals and, in parallel, increased tumor sensitivity to cisplatin chemotherapy [14]. In addition to contrast cancer progression, sodium butyrate was reported to counteract intestinal permeability and mucositis induced in mice by 5-fluorouracil administration [15]. We also recently demonstrated that supplementation of a probiotic blend, ameliorating intestinal damage and other gemcitabine-related adverse effects, was associated with an increase in butyrate-producing bacteria in a mouse model of PDAC [16].

For these reasons and since a decrease in butyrate-producing bacteria has been described in PDAC human patients [17,18], in the present study we explored the effects of sodium butyrate supplementation on pancreatic cancer cells' proliferation, apoptosis and cell cycle, alone and in combination with gemcitabine therapy. M oreover, the effects of butyrate supplementation (with or without chemotherapy) were also investigated in an in vivo PDAC xenograft mouse model.

2. Materials and methods

2.1. Cell culture, sodium butyrate and gemcitabine treatments

Human BxPC-3 and PANC-1 cells were purchased by ATCC. Cells were cultured in RPMI 1640 medium supplemented with 10% fetal bovine serum (FBS), 100 U/mL penicillin and 100 μg/mL streptomycin (Invitrogen Life Technologies, Italy) (henceforth referred to as complete RPMI medium) in 5% CO2 atmosphere at 37 °C. As for PANC-1, cells at passage number between 5 and 9 were used, whereas for BxPC-3 cells at passage number between 19 and 25 were used.

For dose-response assay with sodium butyrate (BUT) (Sigma-Aldrich, Italy), cells seeded in 6-well culture plates were treated with growing concentrations of this compound (0–1–3 mM–5 mM–10 mM) for 48 h. Once determined the half maximal inhibitory concentration (IC50) responsible for 50% cell growth inhibition for each cell line, this was used for further experiments, in the absence or presence of 1 μM gemcitabine (Sigma-Aldrich, Italy) for 48 h.

2.2. Count and viability assay

As first step, BxPC-3 and PANC-1 cells treated with different concentrations of BUT (0–1–3 mM–5 mM–10 mM) for 48 h to determine, for each cell line, the concentration to be used for further experiments. At the end of the treatment, cells were harvested by trypsinization with 0.05% Trypsin-EDTA (1X) (Invitrogen, Life Technologies, Italy) and assayed with the Muse Count and Viability assay kit (Luminex, Austin, Texas), according to the supplier's instructions, in order to determine the number of total cells and the percentage of viable and non-viable cells by loading on Muse Cell Analyzer (Millipore, Italy).

2.3. Cell cycle analysis

BxPC-3 and PANC-1 cells treated as described above were harvested in complete RPMI medium and fixed with 70% cold ethanol and stored at - 20 °C according to the Muse Cell Cycle Kit instructions (Luminex, Austin, Texas). Ethanol-fixed cells mixed with the proprietary reagent containing propidium iodide and RNAse A were incubated for 30 min at room temperature in the dark according to the supplied staining protocol of the kit, before analyzing on Muse Cell Analyzer (Millipore, Italy).

2.4. Apoptosis assay

BxPC-3 and PANC-1 cells treated as described above were assayed for apoptosis at the Muse Cell analyzer by using the Muse Annexin V and Dead Cell Assay kit (Luminex, Austin, Texas), accordingly to the supplier's instructions. Briefly, a cell suspension was incubated with an equal volume of Muse Annexin V & Dead Cell Reagent for 20 min in the dark, before analyzing on the Muse Cell Analyzer.

2.5. Animal studies

The in vivo study was authorized by the Italian Ministry of Health, with the approval number 210/2019-PR. 1×10^6 BxPC-3 human cells were subcutaneously injected in the flank of twenty 5–6 weeks old female nude BALB/c mice. Once tumors reached an average volume of 100 mm^3 (21 days after cells inoculation), mice were randomly assigned to the following experimental groups (5/group): CTRL (control), GEM (50 mg/kg gemcitabine intraperitoneally once a week), BUT (800 mg/kg sodium butyrate for five consecutive days/week by gavage.), GEM+BUT (50 mg/kg/week gemcitabine i.p. and 800 mg/kg sodium butyrate for five consecutive days/week by gavage). Animals had free access to food and water and were monitored daily for sign of illness. Body weight and tumor volume was measured twice/week. After four weeks of treatment, blood was collected from the mandibular plexus, fresh fecal pellets were harvested from the cages and both were stored at − 80 °C. Upon sacrifice by CO_2 inhalation, tumors and intestines were explanted and were formalin- fixed for histological analyses.

2.6. Histological and immunohistochemical analyses

For histopathological and immunohistochemical analyses mouse tissues were fixed in 4% paraformaldehyde (PFA) and paraffin embedded with Diapath automatic processator. To assess histological features Haematoxylin/Eosin (Diapath) staining was performed according to standard protocol and samples were mounted in Eukitt (Bio-Optica). Masson's Trichrome staining (Diapath, 010210) and Picrosirius Red staining (Scy Tek Lab, SRS-IFU) were performed and visualized under a bright-field microscope and a polarized light (Olympus Upright BX63) to show collagen specificity. Histological visualization of intestinal mucins was performed using Alcian Blue pH 2.5/Periodic acid-Schiff (PAS) staining (Bioptica 04–163802). For immunohistochemical (IHC) analysis paraffin was removed with xylene and the sections were rehydrated in graded alcohol. Antigen retrieval was carried out using preheated target retrieval solution for 30 min. Tissue sections were blocked with 2% FBS serum in PBS for 60 min and incubated overnight with the following primary antibodies: Ki67 (Thermofisher, MAB-14520, 1:50), α-SMA (Sigma-Aldrich, A5228, 1:400), IBA1 (Wako, 019–19741, 1:100), F4/80 (Cell Signaling, 70076, 1:250), Arginase 1 (Gene Tex, GTX109242, 1:200), CD206 (Abcam, ab64693, 1:4000), Collagen IV (Bio-Rad, 2150–1470, 1:200), Podocalyxin (R&D Systems, AF1556, 1:200).

The antibody binding was detected using a polymer detection kit (GAM/GAR-HRP, Microtech) followed by a diaminobenzidine chromogen reaction (Peroxidase substrate kit, DAB, SK-4100; Vector Lab). All sections were counterstained with Mayer's hematoxylin and

visualized using a bright-field microscope. For double immunofluorescence, tumor sections were incubated overnight with primary antibodies and then incubated with corresponding secondary antibodies Alexa Fluor 488 or 594 (1:200, Molecular Probes, Invitrogen Life Technologies, Grand Island, New York) for 1 h at room temperature. To visualize the cell nuclei, human specimens were counterstained with 4,6-diamidino-2-phenylindole (DAPI, Sigma-Aldrich), mounted with a Phosphate-Buffered Salines/glycerol solution and examined under a Leica TCS SP2 confocal microscope. A custom Fiji plugin [19] was used to extract the area positive either for the Collagen in Masson Trichrome staining or the aSMA positive area. In order to segment the positive areas, the acquired RGB (red, green and blue) images were first converted to HSB (hue, saturation and brightness) images. Then, the channels were separated and the following thresholds were applied, respectively for Masson Trichrome and aSMA: Hue, from 151 to 212 and from 0 to 70; Saturation, from 40 to 255 and from 25 to 255; Brightness, from 0 to 227 and from 0 to 255. The resulting segmented images were then combined using the AND operator to obtain a single, segmented, image. After the segmentation, the positive areas were identified using the analyze particles plugins with neither size nor circularity selection. The identified particles (ROIs) showing a mean Hue higher than 204 and 150, respectively for Masson Trichrome and aSMA, were excluded from the further analysis. Finally, to exclude the unstained areas within the fibers, the area surrounding the ROIs was cleared and a new selection was generated based on the resulting image. This new selection was finally used to extract the area.

2.7. 16S rRNA gene sequencing and analysis

DNA was isolated from mice fecal samples using the QIAamp DNA Stool Mini Kit (Qiagen) according to the manufacturer's instructions to optimize the ratio of microbial to host DNA. Libraries of the V3-V4 hypervariable region of bacterial 16 S rRNA gene were prepared and sequenced as previously described [20] on an Illumina MiSeq device (Illumina Inc).

FASTQ files were analyzed by the 16 S Metagenomics GAIA 2.0 tool (http://www.metagenomics.cloud, Sequentia Biotech, Barcelona, Spain, 2017), which performs the quality control of the reads/pairs (i.e., trimming, clipping and adapter removal) through FastQC and BBDuk. The reads/pairs are mapped with BWA-MEM against the custom databases (based on NCBI).

2.8. Serum biochemical profile in mice

In order to assess whether butyrate supplementation had any effect on serum biochemical profile of mice, blood was collected shortly before sacrifice and hepatic and renal serum markers were analyzed (Table 1).

Table 1
Gemcitabine and/or butyrate treatment impact on serum biochemical parameters.

	CTRL	GEM	BUT	GEM + BUT
AST (u/L)	361.00 (± 171.53)	284.67 (± 235.87)	116.50 (± 40.86) *	151.00 (± 24.04)
ALT (u/L)	132.00 (± 43.01)	69.00 (± 14.18)	69.25 (± 42.20)	69.75 (± 12.66)
ALP (u/L)	94.50 (± 26.15)	88.33 (± 41.36)	120.75 (± 68.45)	118.75 (± 29.24)
GGT (u/L)	23.25 (± 14.93)	14.00 (± 6.08)	15.75 (± 5.06)	17.25 (± 12.42)
Urea (mg/dL)	159.50 (± 44.29)	70.67 (± 17.62)*	53.75 (± 5.50)**	68.00 (± 23.37)
Creatinine (mg/dL)	1.04 (± 0.12)	0.91 (± 0.24)	1.05 (± 0.10)	0.99 (± 0.03)
Phosphorus (mg/dL)	11.80 (± 1.34)	12.68 (± 0.80)	12.40 (± 0.45)	11.90 (± 0.67)

* Significant vs CTRL, $p < 0.05$.
** Significant vs CTRL, $p < 0.01$.

2.9. Serum metabolomics

Three types of metabolome profiling were performed on serum samples: *a)* small and highly polar metabolites, *b)* medium polar metabolites and *c)* lipidome. The serum and Quality Control (QCs) samples were extracted with use of Ostro 96 well plates (Waters) allowing for separation of small molecules fraction from phospholipids fraction. Small molecule fraction was aliquoted in two vials: one dedicated to analysis on reverse phase chromatographic column C18, and the second one on BEH Amide HILIC chromatographic column, covering highly polar and medium polar metabolites respectively. Fraction containing phospholipids was analyzed on BEH C8 chromatographic column as for lipidome profiling. Each biological replicate was analyzed in technical triplicate. Details regarding mobile phases and mass spectrometry conditions are provided in Supplementary Fig. S2. Annotation of statistically significant metabolites was performed against in-house library, while remaining unknown compounds underwent the meticulous manual structure elucidation process.

2.10. Processing of metabolomics data

The raw.wiff files were converted into.abf with use of ABF Converter and analyzed by MS-DIAL software. The MS-DIAL analysis were performed separately for each of the three metabolomics assays, separately for positive and negative ionization modes. For normalization of samples, the LOWESS approach was used, available within MS-DIAL software [21].

2.11. Statistics

Data are presented as mean ± standard deviation. *In vitro* experiments were performed at least in triplicate. Student *t*-test was used to compare means in pairwise comparisons. Results were considered significant when $p < 0.05$(*), $p < 0.01$(**), $p < 0.001$(***). As for differential analysis of taxonomic data, DESeq2 statistics was performed and results were considered significant when $p < 0.05$ and FDR< 0.05. ANOVA statistical test corrected for FDR was applied to metabolome profiling data.

3. Results

3.1. Butyrate inhibits in vitro pancreatic cancer cells' growth

For both BxPC-3 and PANC-1 cell lines, the dose-response assay revealed that higher percentages of growth inhibition were observed as BUT concentration increased from 1 mM to 3 mM, 5 mM and 10 mM (75.58% ± 0.46%, 49.84% ± 2.81%, 35.00% ± 3.76%, 24.57% ± 0.05% for BxPC-3% and 69.04% ± 3.52%, 47.07% ± 0.22%, 36.30% ± 4.44%, 34.38% ± 6.09% for PANC-1, respectively) (Fig. 1A). On the other hand, the assessment of cell viability did not reveal any significant change compared to the control (Fig. 1B). The online software application "APA AAT Bioquest, Inc." was used to calculate the IC50 for butyrate in each cell line. As shown in Fig. 1C-D, the calculated IC50 was 1.2 mM for BxPC-3 and 2.3 mM for PANC-1. These concentrations were used from then on. Subsequently, BxPC-3 (Fig. 1E) and PANC-1 (Fig. 1F) were treated with GEM or BUT alone and with a combined treatment (GEM+BUT), to evaluate the effect on growth inhibition. In both cell lines, all three treatments significantly inhibited cell growth when compared to the CTRL (GEM 12.84% ± 1.90%, BUT 58.61% ± 0.91%, GEM+BUT 7.36% ± 1.91% in BxPC-3; GEM 13.59% ± 2.01%, BUT 42.33% ± 6.09%, GEM+BUT 6.23% ± 0.64% in PANC-1). Interestingly, GEM+BUT treatment induced a further statistically significant decrease with respect to GEM alone.

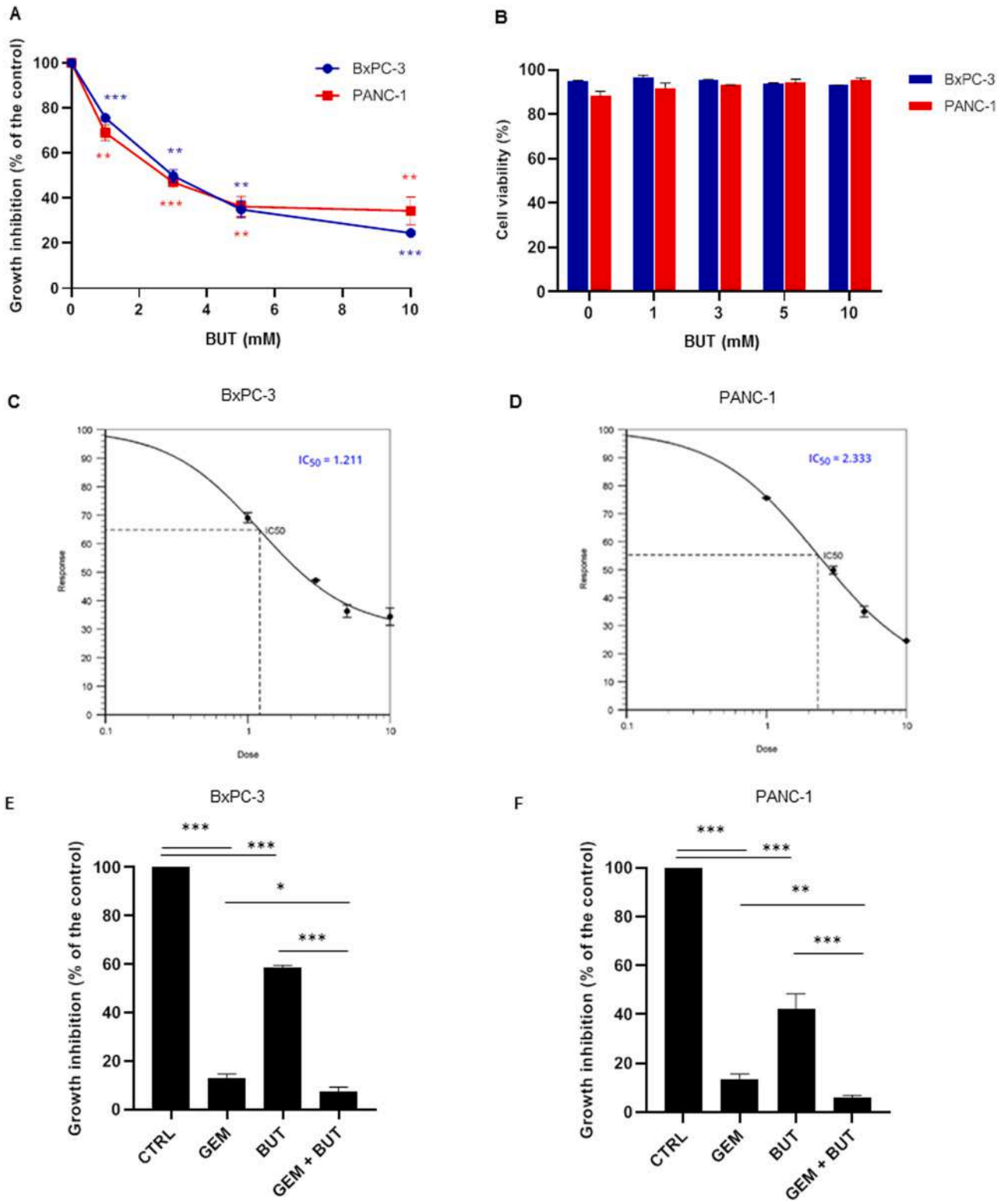

Fig. 1. *In vitro* effect of butyrate with and without gemcitabine on cell growth and viability in pancreatic cancer cell lines. Butyrate-induced dose-response inhibition of cell growth in BxPC-3 and PANC-1 cell lines (A). Butyrate-induced dose-response effect on viability in BxPC-3 and PANC-1 cell lines (B). IC50 value of butyrate for BxPC-3 (C) and PANC-1 (D) cell lines. Cell growth inhibition induced by gemcitabine and/or butyrate treatment in BxPC-3 (E) and PANC-1 (F) cell lines. Data are expressed as means ± SD of at least three independent experiments. Differences were considered significant when $p < 0.05$ (*), $p < 0.01$ (**) or $p < 0.001$ (***).

3.2. Gemcitabine, butyrate and combined treatment affect cell cycle especially in PANC-1 cell line

In order to assess whether cell growth inhibition upon GEM and/or BUT treatment was due to alterations in cell cycle progression, BxPC-3 and PANC-1 cells were subjected to cell cycle analysis. Results are shown in column charts in Fig. 2A-B, respectively.

As concerns BxPC-3, the only significant change in cell cycle

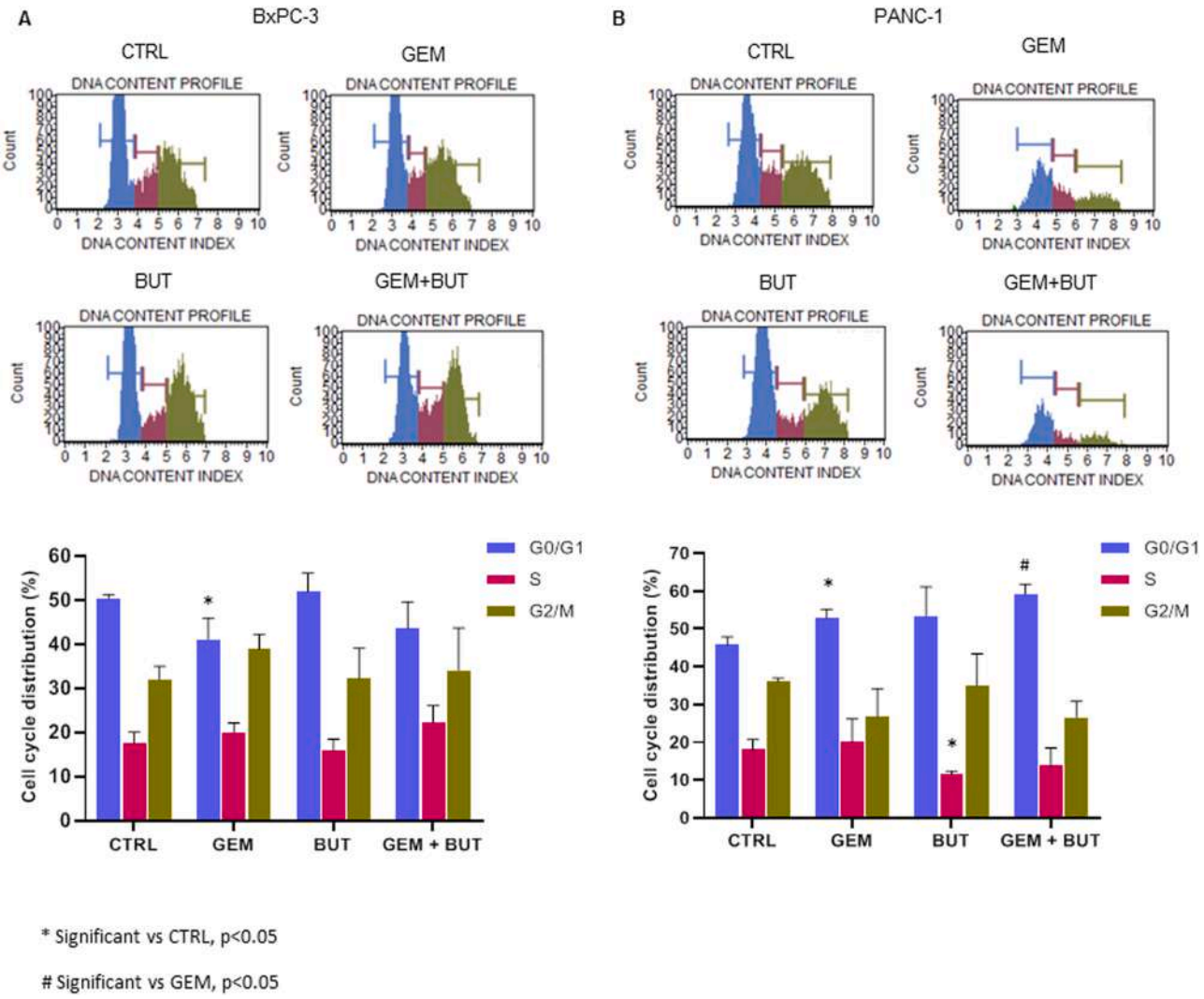

Fig. 2. *In vitro* effect of gemcitabine and/or butyrate treatment on cell cycle in pancreatic cancer cell lines. Representative plots and relative quantification of cell cycle progression after 48 h of treatment, with gemcitabine and/or butyrate in BxPC-3 (A) and PANC-1 (B) cell lines. Data are expressed as means ± SD of at least three independent experiments. Differences were considered significant versus the CTRL when $p < 0.05$ (*). Differences were considered significant versus GEM when $p < 0.05$ (#).

progression was the decrease in G0/G1 phase induced by GEM, whereas no significant change was observed when treating with BUT and GEM+BUT. On the contrary, in PANC-1 cell line, GEM treatment caused an increase in G0/G1 phase compared to the CTRL. A further rise in G0/G1 abundance was observed when GEM+BUT was compared to GEM. In addition, BUT significantly decreased the percentage of cells in S-phase relative to CTRL.

3.3. Butyrate combined treatment accentuates gemcitabine-induced apoptosis in pancreatic cancer cells

We next sought to investigate whether apoptosis was induced in the four experimental conditions. Fig. 3A-B shows representative plots of the apoptosis assay performed on BxPC-3 and PANC-1, respectively.

With regard to BxPC-3, in comparison with CTRL, a statistically significant reduction of live cells was observed upon GEM treatment with simultaneous significant increase in early apoptotic and in total apoptotic cells. No significant variation was detected in cells treated with BUT with respect to CTRL. Differently, when GEM+BUT was compared to GEM treatment, a significant reduction in the percentage of live cells and a concomitant increase in total apoptotic cells was observed. In this condition, early and late apoptotic cells did not show statistically significant changes. Finally, in the comparison between GEM+BUT and BUT treatments, live cells were significantly reduced whereas early, late ant total apoptotic cells were increased (Fig. 3A).

Similarly, in PANC-1 cell line, a statistically significant reduction of live cells and a simultaneous significant increase in early, late and total apoptotic cells was observed in GEM, when compared to CTRL. A significant increase of cells in early apoptosis was found in BUT compared to CTRL. Furthermore, GEM+BUT treatment lowered the percentage of live cells while increasing that of early, late and total apoptotic cells either in comparison with GEM and with BUT single treatments (Fig. 3B).

3.4. Butyrate alone and combined with gemcitabine decrease stromatogenesis in mouse tumor tissues

We then evaluated the effects of butyrate alone and in combination with gemcitabine in a xenograft pancreatic cancer mouse model. Animals were treated according to the protocol summarized in Fig. 4A. In mice treated with gemcitabine-based and butyrate-based single treatments and with the combined treatment, tumor volumes at the end of the protocol were not significantly different (Fig. 4B).

When analyzing tumor histology, nests and sheets of tumor cells

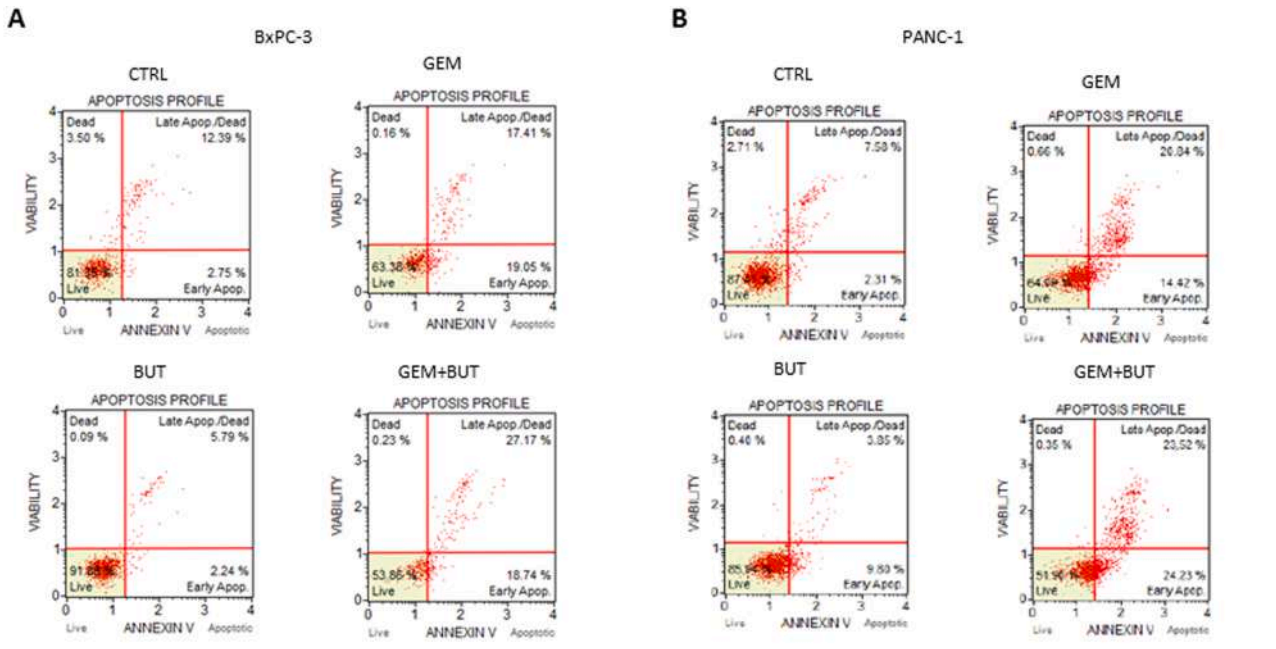

	Live	Early apoptotic	Late apoptotic	Total apoptotic
CTRL	79.2 ± 9.4	2.4 ± 0.4	15.5 ± 9.5	17.9 ± 9.2
GEM	* 64.9 ± 4.6	** 20.0 ± 6.5	14.6 ± 2.9	* 34.6 ± 4.6
BUT	88.4 ± 7.2	5.9 ± 5.6	5.3 ± 2.0	11.2 ± 7.3
GEM + BUT	## ††† 54.7 ± 1.5	†† 24.0 ± 6.1	†† 21.0 ± 5.3	## ††† 45.0 ± 1.8

	Live	Early apoptotic	Late apoptotic	Total apoptotic
CTRL	88.9 ± 5.4	1.6 ± 0.8	6.9 ± 4.5	8.5 ± 5.2
GEM	* 74.1 ± 11.1	** 9.2 ± 4.8	* 15.6 ± 6.5	* 24.8 ± 11.2
BUT	85.8 ± 3.9	*** 7.9 ± 2.7	5.7 ± 1.9	13.6 ± 4.0
GEM + BUT	## ††† 50.3 ± 11.2	## †† 25.4 ± 9.3	# ††† 27.3 ± 7.8	## ††† 49.3 ± 11.2

*Significant vs CTRL, p<0.05
** Significant vs CTRL, p<0.01
*** Significant vs CTRL, p<0.001
# Significant *vs* GEM, p<0.05
Significant *vs* GEM, p<0.05
†† Significant *vs* BUT, p<0.01
††† Significant *vs* BUT, p<0.001

Fig. 3. *In vitro* effect of gemcitabine and/or butyrate treatment on apoptosis in pancreatic cancer cell lines. Representative plots and relative quantification of live, early apoptotic, late apoptotic and total apoptotic cells after 48 h of treatment with gemcitabine and/or butyrate in BxPC-3 (A) and PANC-1 (B) cell lines. Data are expressed as means ± SD of at least three independent experiments. Differences were considered significant versus the CTRL when $p < 0.05$ (*), $p < 0.01$ (**) or $p < 0.001$ (***). Differences were considered significant versus GEM when $p < 0.05$ (#), $p < 0.01$ (##) or $p < 0.001$ (###). Differences were considered significant versus BUT when $p < 0.05$ (†), $p < 0.01$ (††) or $p < 0.001$ (†††).

were in all the treatment conditions. The tumor cell foci were surrounded by dense collagenic stroma bundles highlighted by Masson's Trichrome and Sirius Red on polarized light, which appeared more dense in CTRL samples, as compared with treated ones. Immunostaining for α-smooth muscle actin (α-SMA) as a marker of myofibroblasts and vascular mural cells highlighted a decreased contribution of these elements to the stromal bundles in the GEM and in combined (GEM+BUT) treatment condition but not in single BUT treatment with respect to CTRL (Fig. 4C). Quantification of stromal stains was provided in Supplementary Fig. S1A-B.

We subsequently focused on vascular architecture as part of the stromatogenesis associated with tumor growth. Double-marker immunofluorescence for Collagen IV and Podocalyxin, vessel associated stromal markers characterizing PDAC [22] and predicting poor prognosis [23], highlighted a reduced expression of the two markers in BUT as compared to CTRL samples, and to a lesser extent, also in combined treatment with respect to chemotherapy alone (Fig. 5). Since tumor-associated macrophages (TAM) are recognized to take part to tumor stroma remodeling and vasculogenesis [24], we also investigated the density of macrophages through IHC for IBA1 and F4/80 markers and M2-associated markers CD206 and Arginase-1. No substantial difference was observed in overall macrophage infiltration among the different groups, as assessed by IBA1 and F4/80 markers. In both BUT and GEM+BUT samples a decrease was observed in pro-tumoral M2-polarized macrophages expressing CD206 and Arginase-1 markers (Fig. 5), when compared with their respective controls. Quantification of macrophage markers was provided in Supplementary Fig. S1C.

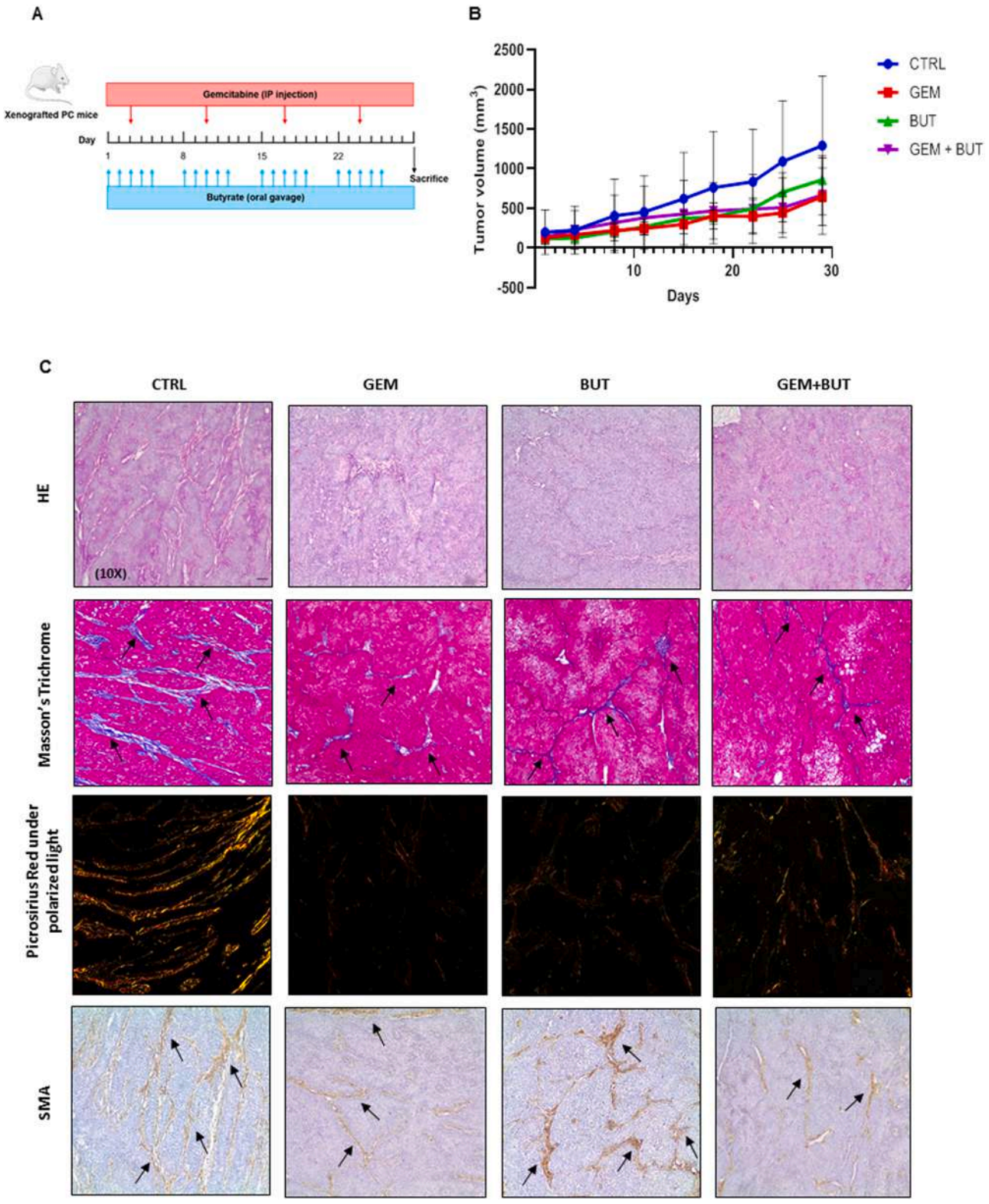

Fig. 4. Impact of gemcitabine and/or butyrate treatment on pancreatic cancer growth and histology. (A) Schematic representation of treatment protocol with gemcitabine and/or butyrate in pancreatic cancer mice. (B) Growth curves obtained by measuring tumor volumes in mice belonging to the different experimental groups. Data are shown as mean ± SD. (C) Histological stain of mouse tumor sections with H&E, Ki67 (brown stain), Masson's Trichrome (blue stain), Picrosirius Red under polarized light (yellow/red stain) and α-SMA (brown stain). All pictures were taken at 10X magnification. Scale bar is 50 μm.

3.5. Butyrate supplementation preserves villi architecture and increases mucin in mouse intestinal sections

Given the well-known role of butyrate in maintaining intestinal functions and in order to evaluate whether its supplementation had any protective effect on chemotherapy-induced gut damage, mouse intestinal sections were analyzed. As depicted in Fig. 6, the overall villi architecture was better preserved in butyrate-supplemented mice as

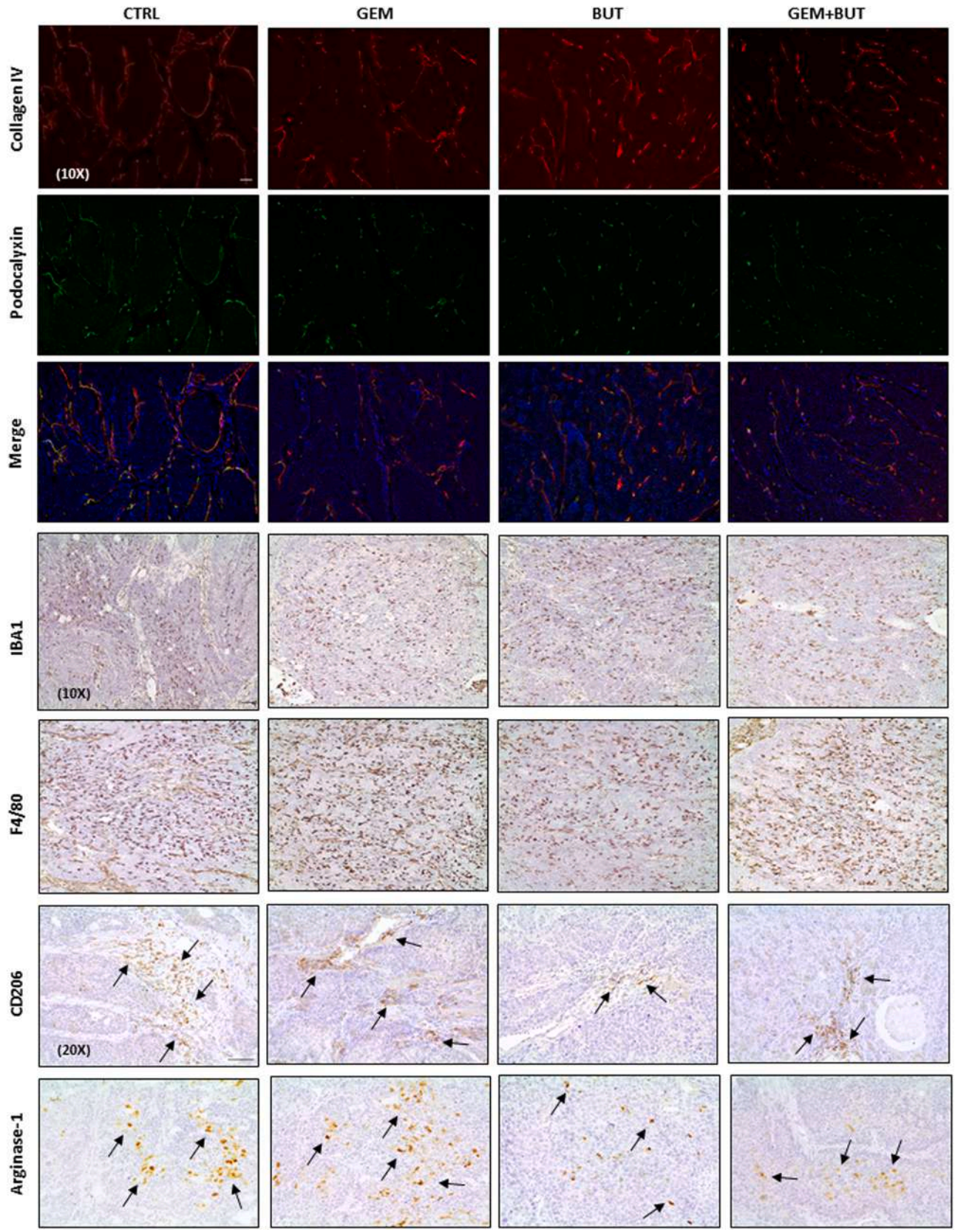

Fig. 5. Impact of gemcitabine and/or butyrate treatment on stromatogenesis. Immunofluorescent stain of mouse tumor tissue sections with Collagen IV (red fluorescence), Podocalyxin (green fluorescence) and merge (10X magnification), showing in butyrate-treated groups as compared to their controls. Immunohistochemical stain with macrophage activation markers Iba1 and F4/80 (10X magnification, brown stain) showing no difference among groups and with M2-macrophage polarization markers CD206 and Arginase-1 (20X magnification, brown stain), showing increased expression in butyrate-supplemented mice compared to their controls. Scale bar is 50 μm.

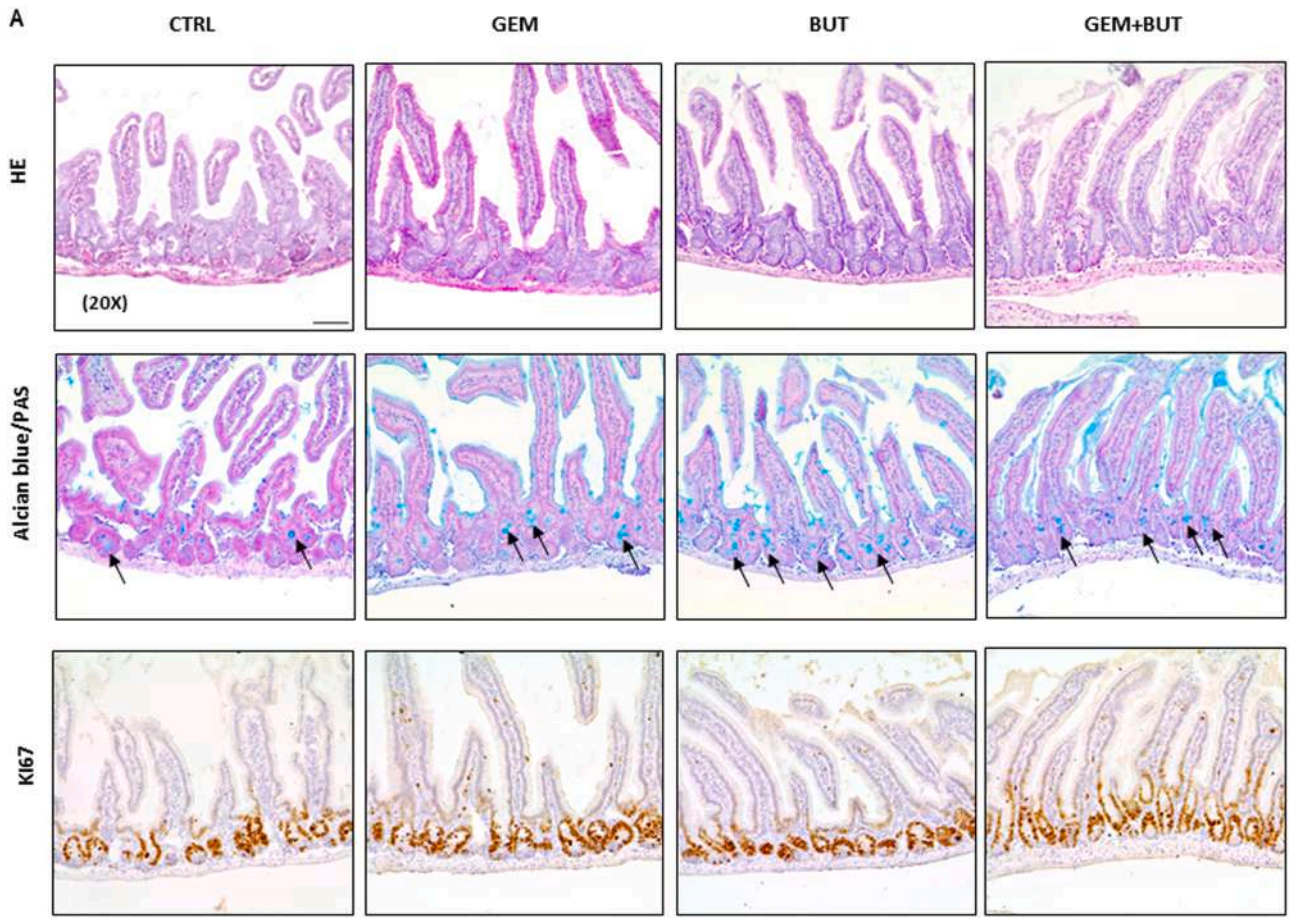

Fig. 6. Gemcitabine and/or butyrate treatment affects intestinal mucosa structure, (A) Histological stain of mouse intestinal sections with H&E, Alcian Blue/PAS (blue stain) and Ki67 (brown stain). Pictures were taken at 20X magnification. Scale bar is 50 μm.

compared to CTRL and GEM mice. In detail, when counting the number of intact villi per field, this was significantly decreased in GEM group with respect to CTRL; on the contrary, it was significantly increased in both BUT and GEM+BUT animals versus CTRL, and in combined (GEM+BUT) treatment as compared to GEM treatment alone (Supplementary Fig. S1D). Likewise, mucin synthesis was significantly increased in butyrate-receiving groups, as indicated by Alcian blue staining (Fig. 6). Quantification of Alcian blue positive cells per crypt was performed, showing a significant increase in all three treated groups compared to CTRL and in combined treatment compared to GEM alone (Supplementary Fig. S1E). Ki67 staining revealed no significant changes in crypt proliferating elements among the different experimental conditions.

3.6. Gemcitabine, butyrate and combined treatment affect gut microbiota composition, structure and function in mice

To explore the effects of the aforementioned treatments on gut microbiota, two fecal pools from each experimental group were subjected to 16 S rRNA gene sequencing. A total of 1628,057 quality-filtered read pairs were obtained, yielding an average of 203,507 read pairs per sample.

The Principal Component Analysis (PCA) plot revealed a clear separation among microbial communities driven by butyrate administration (Fig. 7A). The CTRL and GEM samples are more tightly clustered in the lower left part of the plot, while the two groups supplemented with butyrate are more spread in the remaining part of the plot, indicating that butyrate supplementation introduces a higher variation to the microbial profile. No significant change among the groups was observed when bacterial alpha-diversity was calculated at the species level (Shannon index, Fig. 7B) as well as no relevant change was recorded for species richness (Chao1 index, Fig. 7C).

As for the compositional analysis, an abundance filter was applied to retain only OTUs $> 0.1\%$ of the total abundance per sample.

Firmicutes and *Bacteroidetes* were the most represented phyla in all groups (Fig. 8A) and the *Firmicutes/Bacteroidetes* ratio resulted significantly lower in BUT and GEM+BUT compared to the CTRL, and in BUT versus GEM condition (Fig. 7D). Taxonomy composition revealed interesting differences among the experimental groups. At the phylum level (Fig. 8A), when comparing GEM group with CTRL, *Deferribacteres* (0.78% vs 2.54%) and *Spirochetes* (0.03% vs 0.13%) were found underrepresented. Similarly, in the comparison between BUT and CTRL, *Deferribacteres* (0.60% vs 2.54%) and *Spirochetes* (0.04% vs 0.13%) were found decreased whereas *Actinobacteria* (16.32% vs 10.77%), *Bacteroidetes* (31.32% vs 25.74%), *Proteobacteria* (1.31% vs 1.15%) and *Tenericutes* (4.11% vs 3.64%) were enriched. Combined treatment (GEM+BUT) increased *Deferribacteres* (1.07% vs 0.60%) and *Spirochetes* (0.12% vs 0.03%) as compared to GEM single treatment; *Deferribacteres* were also increased in GEM+BUT relative to BUT (0.12% vs 0.04%), whereas *Tenericutes* were reduced in the same comparison (3.41% vs 4.11%). At the family level (Fig. 8B) *Brachyspiraceae*, *Clostridiaceae*, *Deferribacteraceae* and *Oscillospiraceae* were decreased in GEM compared to CTRL (0.03% vs 0.13%, 7.96% vs 10.24%, 0.59% vs 2.52% and 1.00% vs 1.60% respectively); on the contrary, an increase was recorded for *Erysipelotrichaceae* (0.10% vs 0.03%), *Marinilabiliaceae* (0.20% vs 0.12%) and *Porphyromonadaceae* (1.89% vs 1.37%). When analyzing the family composition in BUT group versus CTRL, *Brachyspiraceae* (0.04% vs 0.13%), *Deferribacteraceae* (0.77% vs 2.52%), *Oscillospiraceae*

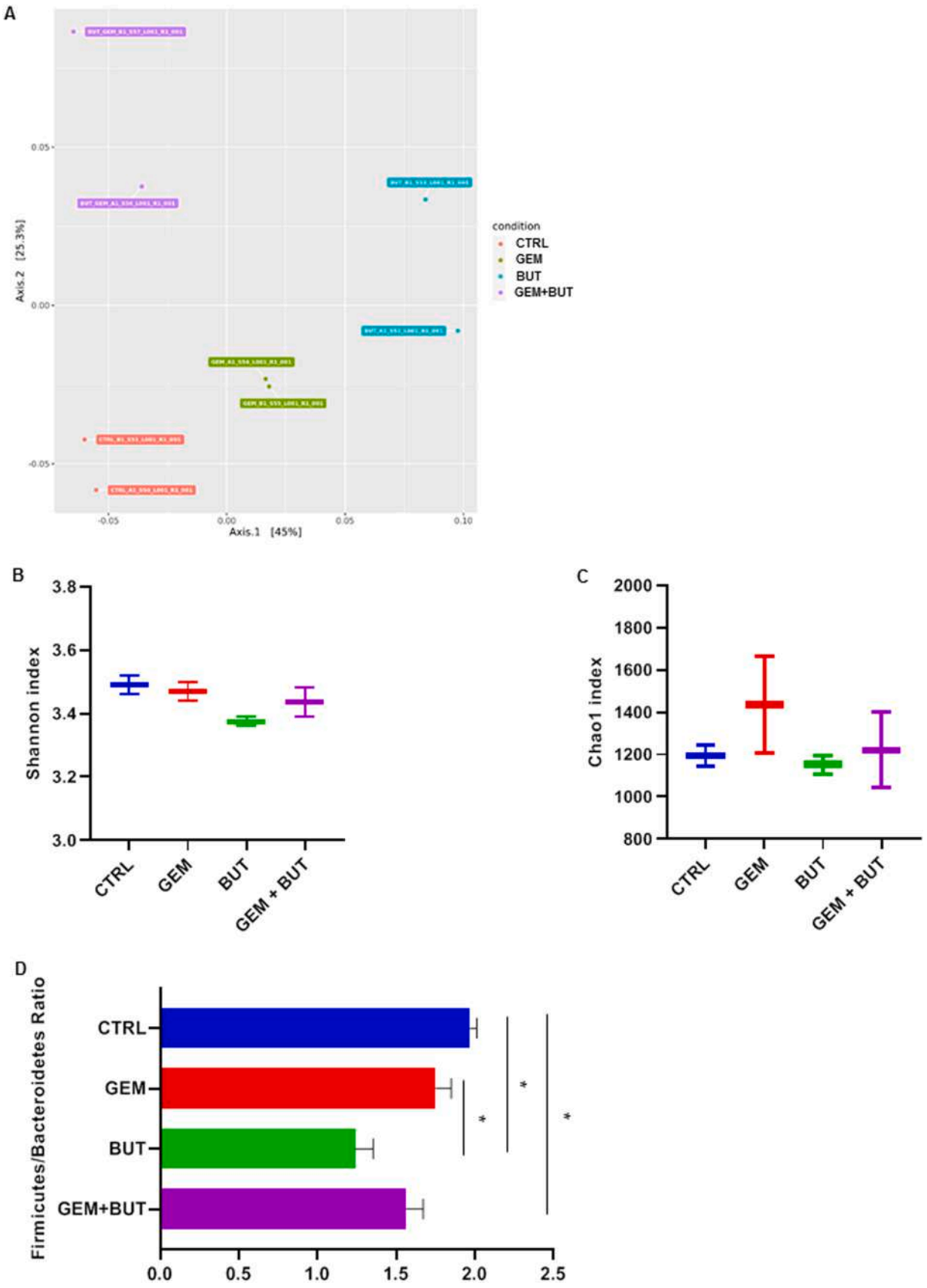

Fig. 7. Effect of gemcitabine and/or probiotic treatment on gut microbiota diversity and composition. PCA plot of the Bray-Curtis distances across the four experimental groups (A). Boxplots representing species-level alpha-diversity expressed by Shannon Index (B) and richness expressed by Chao1 index (C) in the four study groups. *Firmicutes/Bacteroidetes* ratio in the four groups (D). Data are expressed as means of two fecal pools per group. Differences were considered significant when $p < 0.05$ (*).

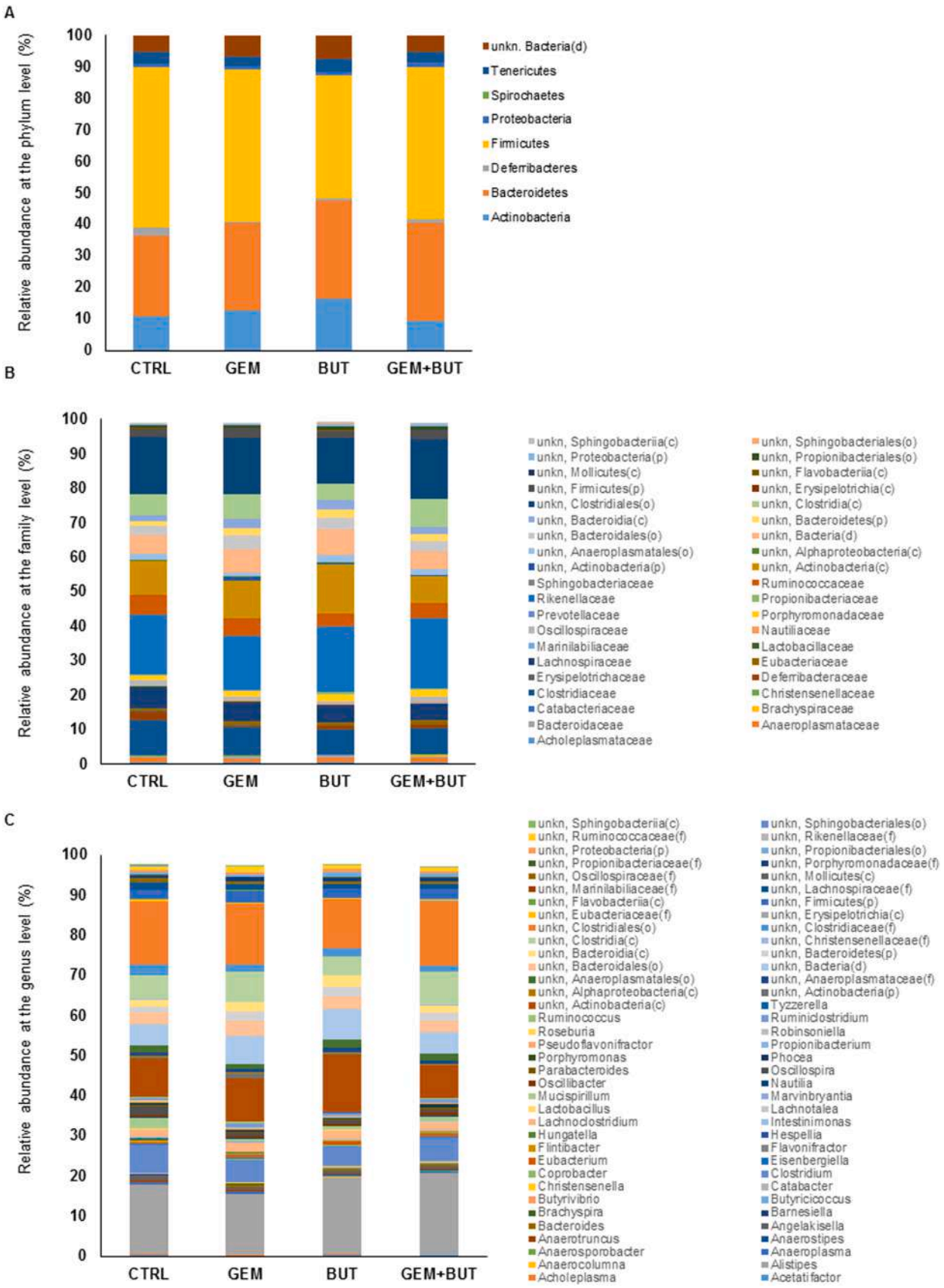

Fig. 8. Effect of gemcitabine and/or probiotic treatment on gut microbiota taxonomic composition. Mean relative abundance of gut bacterial phyla (A), families (B) and genera (C) level. Data are expressed as means of two fecal pools per experimental group.

(0.935% vs 1.60%) and *Ruminococcaceae* (3.40% vs 5.83%) were found under-represented while an increase in *Bacteroidaceae* (0.67% vs 0.26%), *Erysipelotrichaceae* (0.07% vs 0.03%), *Porphyromonadaceae* (1.95% vs 1.37%) and *Propionibacteriaceae* (0.41% vs 0.26%) was observed. When GEM+BUT group was compared to GEM condition, *Erysipelotrichaceae* (0.06% vs 0.10%) and *Lactobacillaceae* (0.03% vs 0.15%) were significantly reduced while *Brachyspiraceae* (0.12% vs 0.03%), *Deferribacteraceae* (1.06% vs 0.59%) and *Propionibacteriaceae* (0.39% vs 0.24%) were over-represented. Similarly, in the comparison between GEM+BUT and BUT *Lactobacillaceae* resulted decreased (0.03% vs 0.12%) whereas *Brachyspiraceae* (0.12% vs 0.04%), *Marinilabiliaceae* (0.24% vs 0.07%) and *Nautiliaceae* (0.28% vs 0.11%) were enriched. Going lower in the taxonomic scale (Fig. 8C) a number of bacterial genera emerged as differentially represented among the experimental groups. Among these, butyrate supplementation caused the enrichment of *Anaerostipes* (0.12% vs 0.09% in BUT vs CTRL), *Bacteroides* (0.64% vs 0.23% in BUT vs CTRL), *Butyrivibrio* (0.09% vs 0.06% in BUT vs CTRL; 0.10% vs 0.08% in GEM+BUT vs GEM), *Eubacterium* (0.68% vs 0.43% in BUT vs CTRL), *Parabacteroides* (0.27% vs 0.18% in BUT vs CTRL; 0.66% vs 0.22% in GEM+BUT vs GEM) and *Propionibacterium* (0.10% vs 0.07% in BUT vs CTRL; 0.09% vs 0.06% in GEM+BUT vs GEM), whereas it decreased the abundance of *Hungatella* (0.003% vs 0.34% in BUT vs CTRL; 0.01% vs 0.17% in GEM+BUT vs GEM), *Lachnotalea* (0.05% vs 0.12% in BUT vs CTRL; 0.07% vs 0.15% in GEM+BUT vs GEM), *Oscillospira* (0.84% vs 2.05% in BUT vs CTRL; 0.57% vs 0.67% in GEM+BUT vs GEM), *Robinsoniella* (0.02% vs 0.14% in BUT vs CTRL) and *Roseburia* (0.10% vs 0.26% in BUT vs CTRL; 0.12% vs 0.21% in GEM+BUT vs GEM).

3.7. Butyrate supplementation lowers the hepatic marker AST and the renal marker urea in mice serum

Interestingly, when assessing the serum hepatic markers, none of the mice in the BUT and GEM+BUT groups had AST levels increased above the reference range (54–269 U/L), while some animals in CTRL and GEM groups did. As a consequence, a notable significant lowering in AST levels was recorded upon BUT treatment (116.50 ± 40.86) compared to the untreated CTRL (361.00 ± 171.53) while a marked though not significant reduction was obtained in GEM+BUT (151.00 ± 24.04) relative to GEM (284.67 ± 235.87). Concerning renal parameters, urea levels were above the reference range (19–27 mg/dL) in all mice whatever the experimental group, as well as the mean value per group of creatinine (reference range 0.3–1.0 mg/dL) and phosphorus (reference range 6.0–10.4 mg/dL), suggesting a kidney damage likely due to cancer. Nevertheless, all the experimental treatments (GEM (70.67 ± 17.62), BUT (53.75 ± 5.50), and GEM+BUT (68.00 ± 23.37)) were able to significantly decrease serum urea levels with respect to the untreated CTRL (159.50 ± 44.29).

3.8. Butyrate supplementation affects mice serum metabolomics, especially lipid profile

We next sought to evaluate whether butyrate administration had any effects on animal serum metabolomics. High number of *m/z* features were found in both metabolome and lipidome profiling dataset, varying between ionization modes. In reverse phase C18 profiling, focused on medium polar metabolites, 5946 and 2177 *m/z* features were detected, respectively in positive and negative ionization mode. On BEH Amide HILIC column, dedicated to the analysis of highly polar metabolites, 3615 and 2200 *m/z* features were found, in positive and negative ionization mode respectively. Finally, in lipidome profiling on BEH C8 column, 8080 and 7643 *m/z* features were detected in positive and negative ionization mode respectively. After application of ANOVA test, the number of *m/z* features of interest, with $p < 0.05$, diminished significantly. Medium polar metabolome profiling brought 912 and 962 statistically significant *m/z* features, respectively in negative and positive ionization modes, highly polar HILIC profiling 709 and 542 features, while lipidome profiling 3077 and 3204. Analysis of PCA plots did not reveal batch effects either shifts in datasets. PCA plots for each chromatographic column and polarity are shown in Supplementary Fig. S3. Differences between the four studied groups were marked strongly in BEH C8 column, especially in negative ionization mode – the four groups were clearly separated. On the other hand, HILIC profiling was found to be less informative, since only GEM group was distinguishable from the rest.

Fig. 9 A shows the score plot from a PCA model calculated on the significantly different features (ANOVA, FDR adjusted $p < 0.05$), including annotated and few unknown but highly significant compounds from all three metabolomics profiling experiments. The BUT samples tended to be close with each other in the lower part of the plot, GEM+BUT samples were found on the left part, while the CTRL and GEM groups were more spread in the remaining part. The abundance of the metabolites differentially represented among the groups according to ANOVA FDR *p* adjusted value, is also shown in the heatmap in Fig. 9B. Besides the names of metabolites, families are marked, to facilitate interpretation. It can be easily seen, a conspicuous perturbation of lipid metabolism upon butyrate treatment turned out. Fatty acids (Fig. 10A), fatty acid metabolites (Fig. 10B) and fatty acid amide metabolites clearly changed in the analyzed groups. In particular, fatty acids amides namely oleamide, palmitamide, eicosenamide, stearamide and oleoylethyl amide exhibited decreasing trend from CTRL – GEM - BUT to GEM+BUT, reaching statistical significance also with paired T-Test: GEM+BUT vs GEM and GEM+BUT vs CTRL (Fig. 10C). Similar trend was observed for hydroxylated fatty acids metabolites namely DiHETE (two isomers), 14-HoDE and 12-HEPE (Fig. 10B). Also in this case besides statistical significance calculated with ANOVA, paired T-Test revealed significance. In addition, a number of triacylglycerols (Fig. 10D) and ceramides (Fig. 10E) were found statistically significant, however increasing or decreasing trends are less clear. Minor changes were observed for other lipid classes of compounds, such as bile acids, phosphatidylcholines and lysophosphatidylethanolamines (Fig. S3).

4. Discussion

The gut microbiota has been associated with many cancers, through several mechanisms which can be summarized into three main functions: i) modulation of host immune system; ii) interaction with host metabolism; iii) direct action of toxins/metabolites produced by microorganisms [25]. Among the bacterial products, butyrate has been recognized to play a major role in microbiota-associated anticancer benefits [26]. The current study revealed sodium butyrate to have a cytostatic effect and demonstrated, for the first time, to enhance gemcitabine-induced growth inhibition, mainly through apoptosis promotion, when tested in vitro on two different human pancreatic cancer cell lines. *In vivo*, in xenografted mice, the tumor volume did not change significantly when sodium butyrate was administered alone or concomitant with gemcitabine chemotherapy. A considerable impact on tumor histology was observed, with butyrate (alone or in combination with gemcitabine) showing a stroma-modulating effect, as demonstrated by decreased levels of ECM, fibrosis, vascular and macrophage markers. These results are intriguing, since stromal cells, ECM, TAMs and blood vessels are all part of the tumor microenvironment, which has a deep influence on tumor biology, progression and response to therapy [27–29]. This is particularly true for PDAC, whose histological hallmark is the presence of a huge amount of stroma surrounding the tumor [29,30]. The stroma-modulating action of sodium butyrate is likely due to its function of histone deacetylases (HDACs) inhibitor and is supported by previous reports of anti-fibrotic effects observed in a chemically-induced rat model of chronic pancreatitis in which butyrate was found to prevent the activation of the pancreatic stellate cells (major responsible of ECM deposition and fibrosis) [31] and in a systemic sclerosis mouse model, in which it was shown to influence macrophage infiltration and

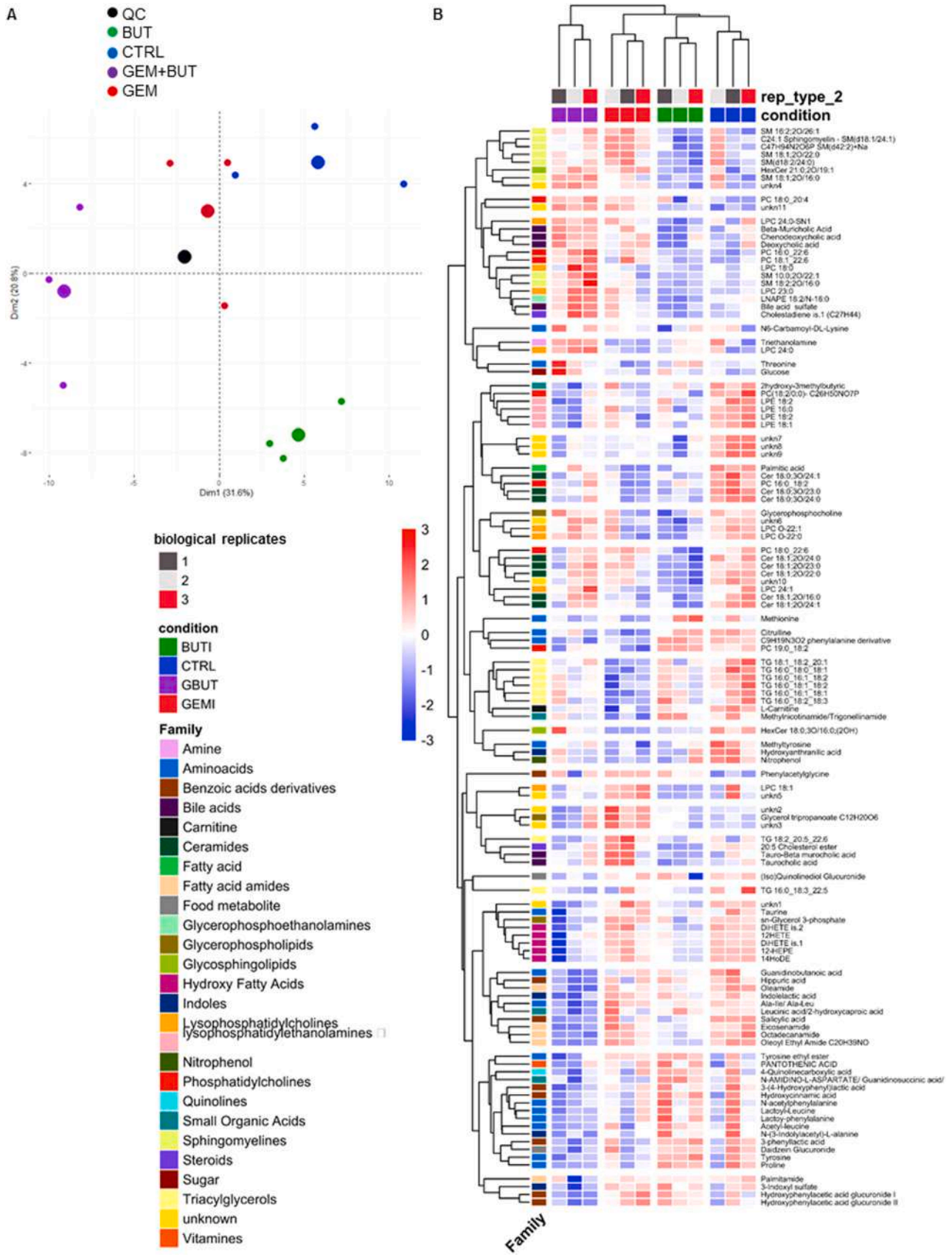

Fig. 9. Gemcitabine and/or butyrate treatment impact on serum metabolomics. (A) Score plot from PCA model calculated on the relative concentrations of the serum significantly different compounds (ANOVA, $p < 0.05$) in the four experimental groups. (B) Heatmap representation of the serum significantly different compounds (ANOVA, $p < 0.05$) in the four groups, including annotated and 4 unknown compounds. Three serum samples per experimental group were assayed in technical triplicates.

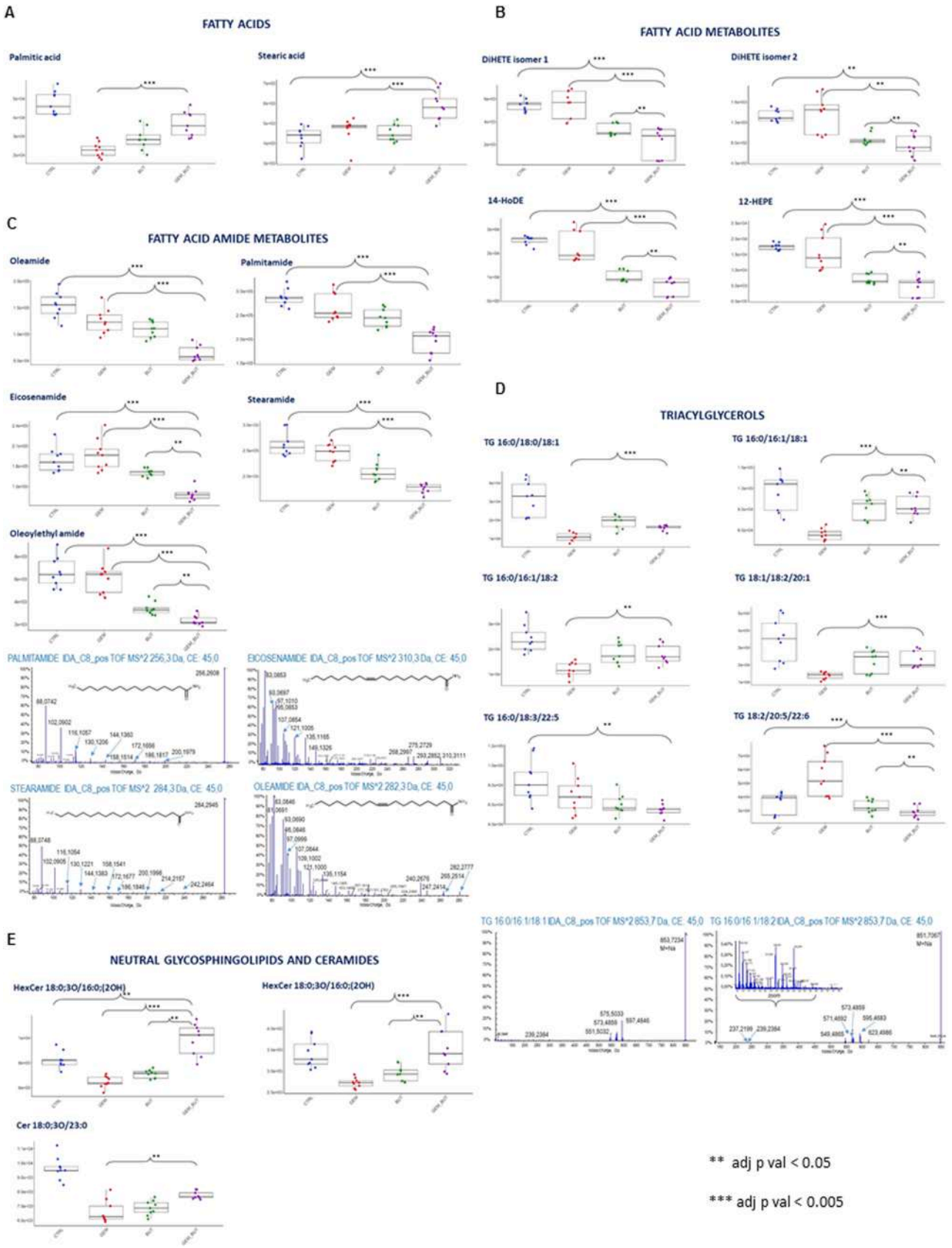

Fig. 10. Alterations in serum lipid profile upon gemcitabine and/or butyrate treatment, Box plots showing the abundance of fatty acids (A), fatty acids metabolites (B), fatty acid amide metabolites (C), triacylglycerols (D) and ceramides (E) in mice'serum samples from the four experimental groups. MS2 fragmentation patterns for fatty acid amide metabolites (C) and triacylglycerols (D) are also shown.

differentiation [32].

As previously observed by we and others with probiotics administration [16,33,34], also the postbiotic sodium butyrate exerted beneficial effects at the intestinal level, preserving gut integrity, ameliorating villi architecture and enhancing mucin production. This effect was particularly relevant when comparing GEM+BUT to GEM group, confirming previous observation that butyrate administration ameliorates chemotherapy-induced gut mucosal damage [15].

Consistent with several previous studies, butyrate administration also remodeled microbiota composition, with *Firmicutes* decreased and *Bacteroidetes* enriched and accordingly reduced *Firmicutes/Bacteroidetes* ratio [13,35,36]. A number of beneficial anti-inflammatory bacteria including butyrate producers (such as *Anaerostipes*, *Butyrivibrio*, *Eubacterium*, *Roseburia*) and propionate producers (i.e *Propionibacterium*) were significantly enriched in animals receiving sodium butyrate alone or combined with gemcitabine when compared to their respective controls. This finding agrees with a previous study demonstrating a role for butyrate administration in increasing butyrate and other SCFAs- producing bacteria in patients suffering from inflammatory bowel diseases [37]. On the other hand, in the same comparisons, some genera associated with gut inflammation, such as *Brachyspira* and *Mucispirillum* [38,39], significantly decreased, in agreement with literature supporting a growth inhibiting effect of butyrate against different pathobionts [40]. In both cases, the microbiota-modulating effect of butyrate can be explained considering that beta-oxidation of butyrate occurring in colonocytes for energy production, consumes oxygen, which in turn sustains the growth of anaerobic butyrogenic bacteria at the expense of pathogenic species [37,40].

Moreover, unlike previous report of no effect on hepatic and renal functionality markers [14], in our mouse model, butyrate administration significantly lowered serum levels of both aspartate aminotransferase (AST) and urea, as compared to untreated controls.

The analysis of serum metabolomics revealed a marked perturbation of lipid metabolism upon butyrate supplementation, which may have potentially impacted on cancer metabolism and progression, given lipids' role as alternative energy sources, cell membrane constituents and signaling molecules to support proliferation of cancer cells. Indeed, SCFAs regulate the balance between fatty acid synthesis, fatty acid oxidation, and lipolysis in the body. Fatty acid oxidation is activated by SCFAs, while de novo synthesis and lipolysis are inhibited [41]. Among the lipid classes significantly changed by butyrate supplementation, the saturated palmitic acid and stearic acid were found increased in GEM+BUT as compared to GEM group. A previous study demonstrated that serum levels of palmitic acid in PDAC patients were much lower than in healthy people [42], whereas another report showed that the dietary intake of both palmitic acid and stearic acid was associated with a lower risk of pancreatic cancer [43]. In parallel with palmitic and stearic acid increase, other fatty acid-related compounds resulted decreased upon butyrate, namely hydroxylated fatty acids and fatty acid amides (FAAs). As also reported in a recent review [44], DiHETEs are known to have pro-inflammatory effects and to be upregulated in several types of cancer, including colorectal cancer, therefore the observed decrease in the GEM+BUT group compared to GEM one, can be indicative of the beneficial effects exerted by butyrate supplementation. The FAAs are signaling lipids of endocannabinoid system and modulate a number of neurobehavioral processes in mammals, including pain, sleep, feeding, and locomotor activity. In tumor cells, several studies have described alterations in endocannabinoid system; however it remains unclear if the endocannabinoid system has an anti- or protumoral role [45–47]. There are scarce data available in blood levels of FAAs in pancreatic cancer patients or pancreas tissues. However at tissue levels several investigations reported downregulation of palmitamide, stearamide, oleamide in endometrial cancer, gastric cancer, lung or hepatocellular carcinoma [48–50]. Concerning blood, higher levels of fatty acid amides with different aliphatic chain length were found in serum samples of lung cancer patients in comparison to healthy controls [51]. Many cancer cells maintain active endogenous lipid synthesis as these are needed for growth, proliferation, redox homeostasis and invasion. Still, the biological functions of FAAs remain to be fully elucidated [52,53]. Other interesting groups of metabolites impacted by BUT supplementation were bile acids and phosphatidylcholines. Primary bile acids in rodents are synthetized from cholesterol through CYP7A1 and CYP27A1 enzymatic activities [54]. In rodents, in hepatocytes, conjugation to taurine occurs and, to very small extent, to glycine. Further transformation to secondary bile acid occurs in the intestine thank to microbiota activities. Interpretation of the levels of bile acids in case of pancreatic cancer under mixed therapy treatment becomes challenging, due to several overlapping factors: i) disease itself impacts bile acid homeostasis, ii) chemotherapy has destructive impact on cancer, but also on host and microbiome, iii) the dietary supplementation with butyrate has its impact on microbiome, which in turn influences bile acid synthesis [55]. As shown in the supplementary Fig. S4, bile acids and phosphatidylcholines families exhibit several similarities. Clearly, treatment with BUT lowered level of bile acids in comparison with GEM, CTRL and GEM+BUT, with exception of taurodeoxycholic acid. This is a known effect, as indeed SCFAs are capable to diminish cholesterol levels in blood, which is the starting point for bile acids synthesis [56]. The proof of concept of this phenomenon can be cholesterol sulfate, a derivative of cholesterol down-represented in the BUT group (Fig. S3). On the other hand, GEM treatment alone increased the levels of bile acids and cholesterol sulfate, in comparison with CTRL group, suggesting altered homeostasis between host-gut microbiome. Such observation is not unexpected, since not only antibiotics but also other kinds of drugs are known to shape microbiota, most likely by inducing changes in gut microenvironment which impact on bacterial growth [57]. As we extensively reviewed elsewhere, a number of chemotherapeutics, including gemcitabine, were documented to produce alterations in gut microbiota composition [58], which may reflect in metabolomics modifications.

We noticed the lack of traces of cholic acid in the serum of all mouse groups, indicating the very strong disease impact on classical, so-called neutral synthesis pathway, which gives rise to cholic acid starting from cholesterol through CYP7A1. Cholic acid is one of the most abundant bile acids in serum mice, thus its absence on the chromatogram is mainly due to altered metabolism rather than machine limit of detection [59]. Interestingly, several taurine bile acids were found in samples, conjugated to cholic acid and deoxycholic acid. These bile acids in free form were not detected in serum, what suggests rapid conjugation rates in the liver. Other isomers of cholic acid, typical for rodents, namely alpha-muricholic acid and beta-muricholic acid were detected very well – See Supplementary Fig. S5A. The latter two bile acids in rodents are primary bile acids, produced through the alternative – acidic synthesis pathway by CYP27A1. Other members of bile acid family not detected in serum samples were ursodeoxycholic acid and lithocholic acid – secondary bile acids – see Fig. S5B. These two metabolites usually are found at low concentration in serum [54], thus their absence could be due to a low limit of detection. Other secondary bile acid – the deoxycholic acid was found in all samples and follows the same trend of other bile acids, however it did not reach statistical significance. This may indicate that microbiome preserved its capacity to transform primary into secondary bile acids. We noted also BUT effect to lower triacylglycerols in comparison with CTRL, which is also in good agreement with literature [56]. We speculate that GEM+BUT joint treatment tends to restore the functionalities of gut microbiome and bile acid homeostasis.

Altogether these findings suggest that accompanying conventional treatments with butyrate supplementation can modify pancreatic cancer biology, alleviate some damages associated to cancer itself or to gemcitabine treatment and, hopefully, enhance clinical outcome.

CRediT authorship contribution statement

Valerio Pazienza: Study concept and design. **Valerio Pazienza,**

Concetta Panebianco, Marynka Ulaszewska, Tiziana Pia Latiano, Annacandida Villani, Annapaola Andolfo, Francesco Perri, Federica Pisati, Adele Potenza: Acquisition, analysis, and interpretation of data. **Claudio Tripodo, Federica Pisati, Fabrizio Orsenigo:** Hystological Analysis. **Valerio Pazienza, Concetta Panebianco, Annacandida Villani:** microbiota experiments. **Valerio Pazienza, Concetta Panebianco, Annacandida Villani:** in vivo and in vitro experiments. **Marynka Ulaszewska, Annapaola Andolfo:** Metabolomic and lipidomic Experiments. **Concetta Panebianco, Marynka Ulaszewska, Fulvia Terracciano, Claudio Tripodo:** Drafting of the manuscript. All authors critically revised the manuscript and approved its final version. All authors have read and agreed to the published version of the manuscript.

Conflict of interest statement

The authors have no competing interest to declare.

Data Availability

Data will be made available on request.

Acknowledgments

This work was supported by "Associazione Italiana Ricerca sul Cancro (AIRC) under IG 2019 – ID. 23006 project – to P.I. Pazienza Valerio" and by Italian Ministry of Health "Ricerca Corrente Programma 2018/2020."

References

[1] P. Rawla, T. Sunkara, V. Gaduputi, Epidemiology of pancreatic cancer: global trends, etiology and risk factors, World J. Oncol. 10 (1) (2019) 10–27.
[2] D. Hariharan, A. Saied, H.M. Kocher, Analysis of mortality rates for pancreatic cancer across the world, HPB 10 (1) (2008) 58–62.
[3] E.E. Merika, K.N. Syrigos, M.W. Saif, Desmoplasia in pancreatic cancer. Can we fight it? Gastroenterol. Res. Pract. 2012 (2012), 781765.
[4] M. Amrutkar, I.P. Gladhaug, Pancreatic cancer chemoresistance to gemcitabine, Cancers 9 (2017) 11.
[5] L. Zitvogel, et al., Anticancer effects of the microbiome and its products, Nat. Rev. Microbiol. 15 (8) (2017) 465–478.
[6] S.J. Lewis, K.W. Heaton, Increasing butyrate concentration in the distal colon by accelerating intestinal transit, Gut 41 (2) (1997) 245–251.
[7] E.J. Bloom, et al., Effect of sodium butyrate, a differentiating agent, on cell surface glycoconjugates of a human pancreatic cell line, Pancreas 4 (1) (1989) 59–64.
[8] B. Farrow, et al., Butyrate inhibits pancreatic cancer invasion, J. Gastrointest. Surg. 7 (7) (2003) 864–870.
[9] F. Natoni, et al., Sodium butyrate sensitises human pancreatic cancer cells to both the intrinsic and the extrinsic apoptotic pathways, Biochim. Biophys. Acta 1745 (3) (2005) 318–329.
[10] R. Bulow, et al., Antifibrogenic effects of histone deacetylase inhibitors on pancreatic stellate cells, Biochem. Pharmacol. 74 (12) (2007) 1747–1757.
[11] M. Kitazono, et al., Effects of a histone deacetylase inhibitor, sodium butyrate, on 53-kDa protein expression and sensitivity to anticancer drugs of pancreatic cancer cells, Curr. Ther. Res. Clin. Exp. 71 (3) (2010) 162–172.
[12] J.C. Encarnacao, et al., Butyrate, a dietary fiber derivative that improves irinotecan effect in colon cancer cells, J. Nutr. Biochem. 56 (2018) 183–192.
[13] X. Ma, et al., Sodium butyrate modulates gut microbiota and immune response in colorectal cancer liver metastatic mice, Cell Biol. Toxicol. 36 (5) (2020) 509–515.
[14] Y. Li, et al., Combining sodium butyrate with cisplatin increases the apoptosis of gastric cancer in vivo and in vitro via the mitochondrial apoptosis pathway, Front. Pharmacol. 12 (2021), 708093.
[15] T.M. Ferreira, et al., Oral supplementation of butyrate reduces mucositis and intestinal permeability associated with 5-fluorouracil administration, Lipids 47 (7) (2012) 669–678.
[16] C. Panebianco, et al., Tuning gut microbiota through a probiotic blend in gemcitabine-treated pancreatic cancer xenografted mice, Clin. Transl. Med. 11 (11) (2021), e580.
[17] Z. Ren, et al., Gut microbial profile analysis by MiSeq sequencing of pancreatic carcinoma patients in China, Oncotarget 8 (56) (2017) 95176–95191.
[18] W. Zhou, et al., The fecal microbiota of patients with pancreatic ductal adenocarcinoma and autoimmune pancreatitis characterized by metagenomic sequencing, J. Transl. Med. 19 (1) (2021) 215.
[19] J. Schindelin, et al., Fiji: an open-source platform for biological-image analysis, Nat. Methods 9 (7) (2012) 676–682.
[20] N. Trivieri, et al., BRAF(V600E) mutation impinges on gut microbial markers defining novel biomarkers for serrated colorectal cancer effective therapies, J. Exp. Clin. Cancer Res. 39 (1) (2020) 285.
[21] H. Tsugawa, et al., MS-DIAL: data-independent MS/MS deconvolution for comprehensive metabolome analysis, Nat. Methods 12 (6) (2015) 523–526.
[22] D. Ohlund, et al., Type IV collagen is a tumour stroma-derived biomarker for pancreas cancer, Br. J. Cancer 101 (1) (2009) 91–97.
[23] K. Saukkonen, et al., Podocalyxin is a marker of poor prognosis in pancreatic ductal adenocarcinoma, PLoS One 10 (6) (2015), e0129012.
[24] R. Afik, et al., Tumor macrophages are pivotal constructors of tumor collagenous matrix, J. Exp. Med. 213 (11) (2016) 2315–2331.
[25] Q. Yu, C. Jobin, R.M. Thomas, Implications of the microbiome in the development and treatment of pancreatic cancer: thinking outside of the box by looking inside the gut, Neoplasia 23 (2) (2021) 246–256.
[26] J. Chen, K.N. Zhao, L. Vitetta, Effects of intestinal microbial(-)elaborated butyrate on oncogenic signaling pathways, Nutrients 11 (2019) 5.
[27] K. Dzobo, C. Dandara, Architecture of cancer-associated fibroblasts in tumor microenvironment: mapping their origins, heterogeneity, and role in cancer therapy resistance, Omics 24 (6) (2020) 314–339.
[28] N.M. Anderson, M.C. Simon, The tumor microenvironment, Curr. Biol. 30 (16) (2020) R921–R925.
[29] F. Polani, P.M. Grierson, K.H. Lim, Stroma-targeting strategies in pancreatic cancer: Past lessons, challenges and prospects, World J. Gastroenterol. 27 (18) (2021) 2105–2121.
[30] D. Xie, K. Xie, Pancreatic cancer stromal biology and therapy, Genes Dis. 2 (2) (2015) 133–143.
[31] G. Kanika, S. Khan, G. Jena, Sodium butyrate ameliorates L-arginine-induced pancreatitis and associated fibrosis in Wistar rat: role of inflammation and nitrosative stress, J. Biochem. Mol. Toxicol. 29 (8) (2015) 349–359.
[32] H.J. Park, et al., Butyrate improves skin/lung fibrosis and intestinal dysbiosis in bleomycin-induced mouse models, Int. J. Mol. Sci. 22 (2021) 5.
[33] M.A. Ciorba, et al., Lactobacillus probiotic protects intestinal epithelium from radiation injury in a TLR-2/cyclo-oxygenase-2-dependent manner, Gut 61 (6) (2012) 829–838.
[34] L.M. Trindade, et al., Paraprobiotic Lacticaseibacillus rhamnosus protects intestinal damage in an experimental murine model of mucositis, Probiot. Antimicrob. Proteins, 2021.
[35] T.J. Oh, et al., Butyrate attenuated fat gain through gut microbiota modulation in db/db mice following dapagliflozin treatment, Sci. Rep. 9 (1) (2019) 20300.
[36] Y.H. Xu, et al., Sodium butyrate supplementation ameliorates diabetic inflammation in db/db mice, J. Endocrinol. 238 (3) (2018) 231–244.
[37] S. Facchin, et al., Microbiota changes induced by microencapsulated sodium butyrate in patients with inflammatory bowel disease, Neurogastroenterol. Motil. 32 (10) (2020), e13914.
[38] Y. Bordon, A microbial trigger for colitis, Nat. Rev. Immunol. 19 (2019) 350–351.
[39] K.S. Jabbar, et al., Association between Brachyspira and irritable bowel syndrome with diarrhoea, Gut 70 (6) (2021) 1117–1129.
[40] J. Chen, L. Vitetta, The role of butyrate in attenuating pathobiont-induced hyperinflammation, Immune Netw. 20 (2) (2020), e15.
[41] G. den Besten, et al., The role of short-chain fatty acids in the interplay between diet, gut microbiota, and host energy metabolism, J. Lipid Res. 54 (9) (2013) 2325–2340.
[42] I.M. Di Gangi, et al., Metabolomic profile in pancreatic cancer patients: a consensus-based approach to identify highly discriminating metabolites, Oncotarget 7 (5) (2016) 5815–5829.
[43] A. Nkondjock, et al., Specific fatty acid intake and the risk of pancreatic cancer in Canada, Br. J. Cancer 92 (5) (2005) 971–977.
[44] B. Wang, et al., Metabolism pathways of arachidonic acids: mechanisms and potential therapeutic targets, Signal Transduct. Target. Ther. 6 (1) (2021) 94.
[45] G. Alpini, S. Demorrow, Changes in the endocannabinoid system may give insight into new and effective treatments for cancer, Vitam. Horm. 81 (2009) 469–485.
[46] T. Ayakannu, et al., The evolving role of the endocannabinoid system in gynaecological cancer, Hum. Reprod. Update 21 (4) (2015) 517–535.
[47] M. Jove, et al., Metabotyping human endometrioid endometrial adenocarcinoma reveals an implication of endocannabinoid metabolism, Oncotarget 7 (32) (2016) 52364–52374.
[48] K. Njoku, et al., Metabolomic biomarkers for detection, prognosis and identifying recurrence in endometrial cancer, Metabolites 10 (2020) 8.
[49] T. Altadill, et al., Metabolomic and lipidomic profiling identifies the role of the RNA editing pathway in endometrial carcinogenesis, Sci. Rep. 7 (1) (2017) 8803.
[50] P. Knapp, et al., Altered sphingolipid metabolism in human endometrial cancer, Prostaglandins Other Lipid Mediat. 92 (1–4) (2010) 62–66.
[51] Y. Li, et al., Serum metabolic profiling study of lung cancer using ultra high performance liquid chromatography/quadrupole time-of-flight mass spectrometry, J. Chromatogr. B Anal. Technol. Biomed. Life Sci. 966 (2014) 147–153.
[52] C. Ezzili, K. Otrubova, D.L. Boger, Fatty acid amide signaling molecules, Bioorg. Med. Chem. Lett. 20 (20) (2010) 5959–5968.
[53] E.K. Farrell, D.J. Merkler, Biosynthesis, degradation and pharmacological importance of the fatty acid amides, Drug Discov. Today 13 (13–14) (2008) 558–568.
[54] M.M. Ulaszewska, et al., Isotopic dilution method for bile acid profiling reveals new sulfate glycine-conjugated dihydroxy bile acids and glucuronide bile acids in serum, J. Pharm. Biomed. Anal. 173 (2019) 1–17.
[55] H.Y. Feng, Y.C. Chen, Role of bile acids in carcinogenesis of pancreatic cancer: an old topic with new perspective, World J. Gastroenterol. 22 (33) (2016) 7463–7477.

[56] Y. Zhao, et al., Structure-specific effects of short-chain fatty acids on plasma cholesterol concentration in male Syrian hamsters, J. Agric. Food Chem. 65 (50) (2017) 10984–10992.
[57] R.K. Weersma, A. Zhernakova, J. Fu, Interaction between drugs and the gut microbiome, Gut 69 (8) (2020) 1510–1519.
[58] C. Panebianco, A. Andriulli, V. Pazienza, Pharmacomicrobiomics: exploiting the drug-microbiota interactions in anticancer therapies, Microbiome 6 (1) (2018) 92.
[59] J.C. Garcia-Canaveras, et al., Targeted profiling of circulating and hepatic bile acids in human, mouse, and rat using a UPLC-MRM-MS-validated method, J. Lipid Res. 53 (10) (2012) 2231–2241.